Hindawi
Advances in Materials Science and Engineering
Volume 2022, Article ID 9391183, 8 pages
https://doi.org/10.1155/2022/9391183

Research Article

Microstructure, Mechanical, and Nanotribological Properties of Ni, Ni-TiN, and $Ni_{90}Cu_{10}$-TiN Films Processed by Reactive Magnetron Cosputtering

Mukesh Kumar [1] **and Ashutosh Sharma** [2]

[1]*Department of Physics, Faculty of Science, Shree Guru Gobind Singh Tricentenary University, Gurgaon, Delhi-NCR, India*
[2]*Department of Materials Science and Engineering, Ajou University, Suwon, Gyeonggi-do 16499, Republic of Korea*

Correspondence should be addressed to Mukesh Kumar; mukesh.kumar@sgtuniversity.org and Ashutosh Sharma; ashu.materials@gmail.com

Received 10 December 2021; Revised 20 January 2022; Accepted 22 January 2022; Published 23 February 2022

Academic Editor: Antonio Caggiano

In this study, nanocrystalline Ni, Ni-TiN, and $Ni_{90}Cu_{10}$-TiN coatings were processed using reactive magnetron cosputtering of Ni, Cu, and Ti targets under Ar and N_2 gas environment. The phase evolution and structure of coatings were analyzed by the X-ray diffraction (XRD) technique. The morphology of the as-prepared nanocomposite films were investigated by high-resolution transmission electron microscopy (HRTEM). The elastic modulus, nanohardness, and scratch resistance of the investigated films were measured using the nanoindentation technique and compared. The results showed that Ni, Ni-TiN and $Ni_{90}Cu_{10}$-TiN coatings exhibited nanocrystalline structure. The $Ni_{90}Cu_{10}$-TiN nanocomposite films showed optimum nanohardness and tribological properties due to the additional TiN additives which enhanced the dispersion hardening of the composite matrix significantly.

1. Introduction

Ni-Ti-based alloys have been widely used in aerospace and biomedical applications due to their attractive biocompatibility, superelasticity, shape memory effect, and oxidation resistance [1–3]. However, poor machinability and wear resistance severely limit the applications of TiNi-based alloys [4]. Due to the advancement of the nanomaterials design and fabrication process, nanoscale composite coatings have received significant recognition in the scientific community because of their excellent specific strength and tribological properties as compared to their bulk counterparts. Specific considerations have been undertaken to study materials processing, microstructure properties relationship of the nanocomposites with either metallic or ceramic matrices. Substantial improvements in composite properties such as microhardness, strength, and wear have been noticed when the average dispersed particle size or matrix grain is reduced to 10–100 nm. Nanocomposite thin films having nanocrystalline (Ti, M) N (M = Al, Si, Zr), [5, 6], TiN [7–10], CrN, or ZrN [11] as the dispersed phase have been widely investigated in amorphous or nanocrystalline Ni matrix to control grain growth and improve composite hardness and toughness. Nanocomposite films also impart minimum compressive residual stress present in the matrix which has been developed with higher hardness and wear resistance in cutting tools and surface protection applications. The nanocrystalline Ni-TiN has been reported to have a low coefficient of friction (COF) as compared to pure TiN films [9, 12]. The TiN films are also considered important materials because of their high hardness and elastic modulus as well as metal-like electrical conductivity [13–15]. However, the adhesion property of the superhard TiN-based coatings is adversely affected by high compressive residual stress developed during their growth [16]. Hence, the integration of Ni-TiN nanocomposite as an interfacial layer between the ceramic coating and the substrates has been recommended to encourage adhesion [17]. Much higher hardness has been

observed for the nanocrystalline Ni films as compared to the coarse grains' microstructure [18–20], as a dislocation-based deformation mechanism effective in the nanocrystalline Ni with grain size varies from 10–20 nm based on in situ tensile straining observed under TEM studies [21, 22]. The presence of ceramic or intermetallic nanoparticles as reinforcement in nanocrystalline metallic matrix stabilizes their microstructure by constraining the growth of the matrix grain during processing or at elevated temperatures [23]. The size distribution of nanosize second phase particles, as well as particle-matrix interfaces, plays a vital role in deciding the mechanical performance of the nanocomposite coatings and is worthy of investigation. A significant number of investigations have been carried out on electrodeposited Ni matrix nanocomposite coatings including Ni-SiC [24], Ni-Al_2O_3 [25], Ni-ZrO_2 [26], and Ni-TiN [27]. Numerous works on electrochemically deposited metal matrix composites have been nicely summarized by Low et al. [28, 29] in their review article. However, in the electrodeposition process, due to presence of electrolytic solution and other reagents, deposited films often get contaminated. Therefore, for the development of nanocomposite thin films with suitable composition, the magnetron sputtering technique can be considered as an accomplished alternative. The details of the magnetron sputter deposition technique and the effect of processing parameters on microstructure have been studied in-depth by Mukesh et al. [30–33]. Additionally, from the literature review, it has been observed that during the processing of the nanocomposite thin films, a huge amount of residual stress developed. Thus, for more practical applications, it is required to minimize the residual stress along with an increase in nanohardness and wear scratch resistance. In this regard, an effort has been made for comparative studies on the microstructure, residual stress, and mechanical and tribological properties of nanocrystalline Ni, (Ni-Ti) N, and $Ni_{90}Cu_{10}$-TiN nanocomposite films developed using reactive magnetron cosputtering under argon plus nitrogen gas environment. Here, Cu was added to achieve a lubrication effect and balance the strength and wear properties. Finally, we compare (Ni-Ti) N and $Ni_{90}Cu_{10}$-TiN coatings with Ni as the reference matrix sample.

2. Experimental Procedure

2.1. Processing. The investigated thin films were processed by a magnetron sputtering system (Model KVS-T 4065, Korea Vacuum Technology, Gyeonggi-do, Korea) under Ar/N_2 gas environment. This system was equipped with two DC power sources and one RF power source for sputtering. Before sputtering of target materials (Ni, Cu, and Ti with 99.9% purity, Sigma Aldrich, Burlington, USA), the chamber was evacuated to a base pressure lower than 2×10^{-6} Torr using a rotary pump and a turbomolecular pump. The thin films were deposited on ultrasonically cleaned (first in acetone and then isopropanol) p-type Si (100) substrates. The parameters used for deposition of the investigated thin films are based on previous work [30], as given in Table 1.

2.2. Characterization. The cosputtered thin films were characterized by grazing incidence X-ray diffraction (GIXRD, Philips X'Pert PRO Diffractometer, Netherlands) for the analysis of grain size and root mean square (RMS) value of strain. During characterization, GIXRD was operated at 40 kV accelerating voltage and 30 mA current. Using Cu K_α radiation (wavelength = 0.154 nm), the GIXRD scans were performed at a grazing angle of 1.5°, in the range between 35° and 65°, at a scanning speed of 0.05°/s. Scherrer equation was used to calculate the grain size and strain developed in the investigated films [33, 34]. The microstructures of these thin films were observed in bright-field (BF) and dark-field (DF) modes under an HRTEM (JEOL JEM 2100, Tokyo, Japan) operated at an accelerating voltage of 200 kV. During microstructural observation, chemical analysis was done by an energy dispersive X-ray spectroscopy (EDX, Oxford, UK). A nanoindenter (TI950 Tribonanoindenter, Hysitron Inc., Minnesota, MN, USA) having Berkovich indenter with a tip radius of ≈50 nm was used for the measurement of elastic modulus and hardness of the investigated thin films. Minimum 25 indentation measurements were done for each investigated film at 0.2 mN/s of loading rate to a maximum load of 2 mN and depths varies in the range of 40–50 nm. The hardness and elastic modulus were determined by analyzing the load-displacement plots obtained from the tests. Important quantities, which can be determined from analysis of load-displacement plots, are peak load (P_{max}) and displacement (h_{max}), the residual depth after unloading (h_f), and slope of the initial portion of the unloading curve, $S = d_p/d_h$, which is known as the elastic stiffness of the contact. The hardness (H) and elastic modulus (E) of the test surface are determined using the relation given by Oliver and Pharr [35–37]. We have used the values of H and E as the combined effect from the substrate and film. Furthermore, to measure the scratch resistance and friction coefficient of the investigated films, using the same instrument and same condition, nanoscratch tests were performed to a length of 20 μm with a lateral speed of 0.5 μm/s.

3. Results and Discussion

3.1. Chemical Composition and X-Ray Diffraction Analysis. The Ni-TiN and $Ni_{90}Cu_{10}$-TiN nanocomposite films compositions have been determined by EDX analysis, and a representative EDX spectrum obtained for the Ni-TiN nanocomposite film is shown in Figure 1. The presence of Si was detected from the Si substrate. These values are the average compositions measured by performing EDX at 5 different locations within the microstructure. The stoichiometric composition of coatings was Ni, Ni-TiN, and $Ni_{90}Cu_{10}$-TiN, respectively. These compositions have been compared with the ratios of separate growth rates of Ni and Cu films deposited using pure Ni and Cu targets, respectively.

The X-ray diffraction patterns of the investigated Ni, Ni-TiN, and $Ni_{90}Cu_{10}$-TiN thin films of thickness in the range of 450 nm to 500 nm are shown in Figures 2(a)–2(c), respectively. The Ni, $Ni_{90}Cu_{10}$, and TiN average grain sizes

Table 1: The deposition parameters for the investigated thin films.

Processing parameters	Values
Base pressure	2.0×10^{-6} Torr
Working pressure	30 m Torr
Gas ratio ($Ar : N_2$)	1 : 2
RF power for Ti target	300 W
DC power for Ni target	50 W
DC power for Cu target	9 W
Substrate temperature	100°C
Substrate bias	−60 V
Speed for substrate rotation	25 rpm
Substrate to target distance	150 mm

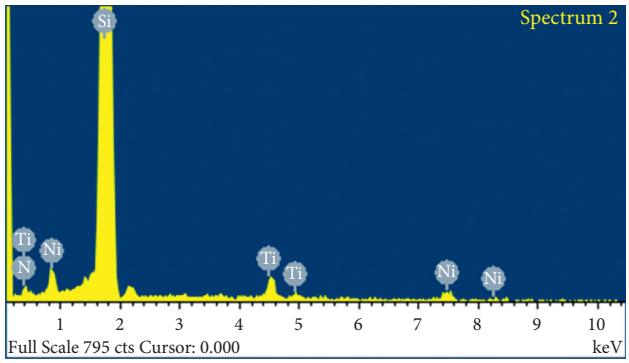

(a)

Figure 1: EDX spectrum obtained for the Ni-TiN nanocomposite film.

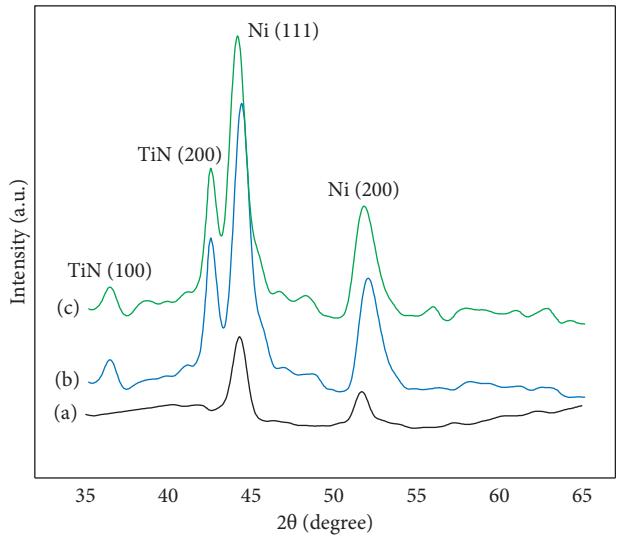

Figure 2: GIXRD patterns of nanocrystalline: (a) Ni, (b) Ni-TiN, and (c) $Ni_{90}Cu_{10}$-TiN thin films.

calculated are given in Table 2. Since there are only two peaks for the particular phase present in the XRD patterns, Williamson Hall plot was not so accurate showing only two data points. Therefore, we used Scherrer equation to calculate the grain size of films [34]. The grain sizes for $Ni_{90}Cu_{10}$ and TiN were lower as compared to the pure Ni. In contrast, the RMS strain for the $Ni_{90}Cu_{10}$-TiN nanocomposite film has been noticed to be higher than the values for Ni and Ni-TiN nanocomposite films.

3.2. Microstructural Analysis. The typical cross-sectional TEM images along with a high-resolution image and a representative selected area electron diffraction (SAED)

Table 2: Crystallite size and RMS strain obtained for Ni, Ni-TiN, and $Ni_{90}Cu_{10}$-TiN thin films.

	RMS strain ($\times 10^{-3}$)	Grain size of Ni and $Ni_{90}Cu_{10}$ (nm)	Grain size of TiN (nm)
Ni	0.8 ± 0.2	19.3 ± 1.3	Not applicable
Ni-TiN	2.4 ± 0.2	13.4 ± 1.2	9.8 ± 1.1
$Ni_{90}Cu_{10}$-TiN	2.8 ± 0.3	13.1 ± 1.6	9.5 ± 1.2

pattern of the Ni, Ni-TiN, and $Ni_{90}Cu_{10}$-TiN nanocomposite films are shown in Figures 3(a)–3(e), respectively. The BF-TEM images of pure Ni show the presence of equiaxed grains (Figure 3(a)). Similar behavior is exhibited by Ni-TiN coatings (Figure 3(b)). To distinguish the TiN in Ni matrix, we performed a comparison of BF and DF-TEM images, as shown in Figures 3(d) and 3(e). A sharp interface between the two phases without any amorphous region is noticed (Figures 3(d) and 3(e)). This is also confirmed by the absence of diffuse halo in the SAED pattern (Figure 3(f)). The circular rings present in the SAED pattern reveal the presence of both Ni and TiN phases. The SAED pattern reveals the presence of both Ni and TiN phases. Furthermore, the particle size of Ni, $Ni_{90}Cu_{10}$, and TiN films was measured using BF and DF images. These measured values of particle sizes match the results obtained by the GIXRD.

3.3. Nanoindentation Elastic Modulus and Hardness. The load versus indentation depth plots for the $Ni_{90}Cu_{10}$-TiN nanocomposite films are shown in Figure 4(a), and the corresponding image depicting a typical array of Berkovich indentations is shown in Figure 4(b). In Figure 4(a), the main parameters during the indentation test are maximum depth, final depth, and load are shown. The elastic and plastic energy can be given by We and Wp, respectively [38, 39].

$$\begin{aligned} &\text{Total energy Wt} = \text{Wp} + \text{We} \\ &\text{According to the power law function, } P = \beta\, h^2 \text{ (loading), and} \\ &P = \alpha\,(\text{hmax-hfinal})n \text{ (unloading),} \end{aligned} \tag{1}$$

Where P is the load, and α and n are the material constants determined from regression analysis. The β is a material constant that depends upon the elastic and plastic properties of the material. According to the measure of the resistance to plastic deformation, we can estimate the plastic energy as the irreversible energy of the indentation, which can be correlated with the value Wp/Wt. Furthermore, the bar charts depicting the ratios of plastic work of the indentation (W_p) to total work of indentation (W_t) indicate that the trend followed is as follows: Ni > Ni-TiN > $Ni_{90}Cu_{10}$-TiN films, as shown in Figure 4(c). This result confirms that the amount of plastic work done during nanoindentation is increased with a decrease in the hardness of the films, irrespective of their compositions. In addition, both elastic modulus and hardness obtained by nanoindentation tests on the aforementioned thin films are shown in Figure 4(d). On examination of the results shown in both Figures 4(c) and 4(d), the values of W_p/W_t are found to increase with a decrease in the hardness value of the investigated film. This result confirms that the amount of plastic work done during nanoindentation is increased with a decrease in the hardness of the present investigated films, irrespective of their compositions.

The results shown in Figure 4(d) also show that both hardness and elastic modulus for the nanocomposite thin films are significantly higher than that of nanocrystalline Ni. On alloying, the hardness values increase due to solid solution hardening, whereas in the case of the composite, the second phase particles act as obstacles for dislocation motion, and consequently, the strength is enhanced. Hardness enhancement is also probably due to the combined effects of the increase in the root mean square (RMS) strain as well as compressive residual stress observed on alloying with Cu and the addition of TiN as reinforcement.

3.4. Nanotribological Properties. Typical AFM images showing the nanoindentation scratches in nanocrystalline Ni-TiN and $Ni_{90}Cu_{10}$-TiN thin films deposited at optimized conditions are shown in Figures 5(a) and 5(b), respectively. After the inspection of scratch surfaces, there is evidence of displacement of material from inside [40–43]. Bar charts showing the variation of width and depth of the nanoindenter-made scratches on Ni, Ni-TiN, and $Ni_{90}Cu_{10}$-TiN nanocomposite films are shown in Figure 5(c). The results present in this figure indicate that the values of depth and width of scratch are much smaller for the nanocomposite films compared to those found for pure Ni films. The enhancement in scratch resistance of the present investigated films due to alloying of the matrix with Cu is only marginal.

The COF versus lateral displacement graph is shown in Figure 5(d). It shows that (i) the values of COF vary in the range of 0.3–0.5, (ii) the average COF decreases in the following order: Ni < Ni-TiN < $Ni_{90}Cu_{10}$-TiN, and (iii) with an increase in lateral displacement, the more or less stable value of COF is observed in case of the $Ni_{90}Cu_{10}$-TiN nanocomposite film, whereas large fluctuations are being observed for the other films. It is a fascinating result that for a given lateral displacement of the indenter, the value of COF

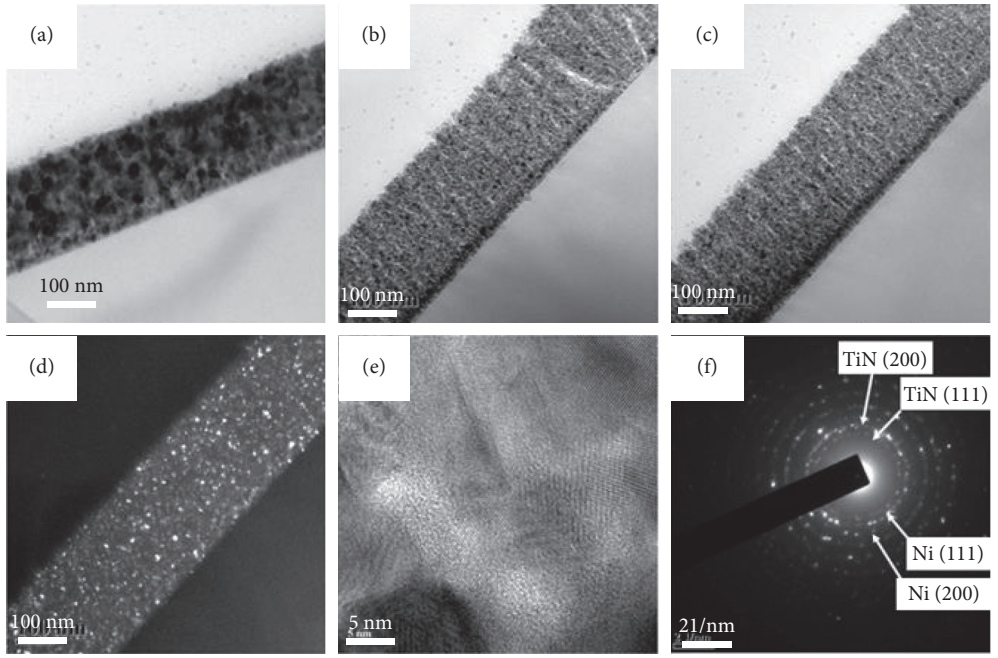

FIGURE 3: (a–c) BF-TEM images of Ni, Ni-TiN, and $Ni_{90}Cu_{10}$-TiN, (d) DF-TEM image of $Ni_{90}Cu_{10}$-TiN, (e) high-resolution image of $Ni_{90}Cu_{10}$-TiN, and (f) SAED pattern of (e).

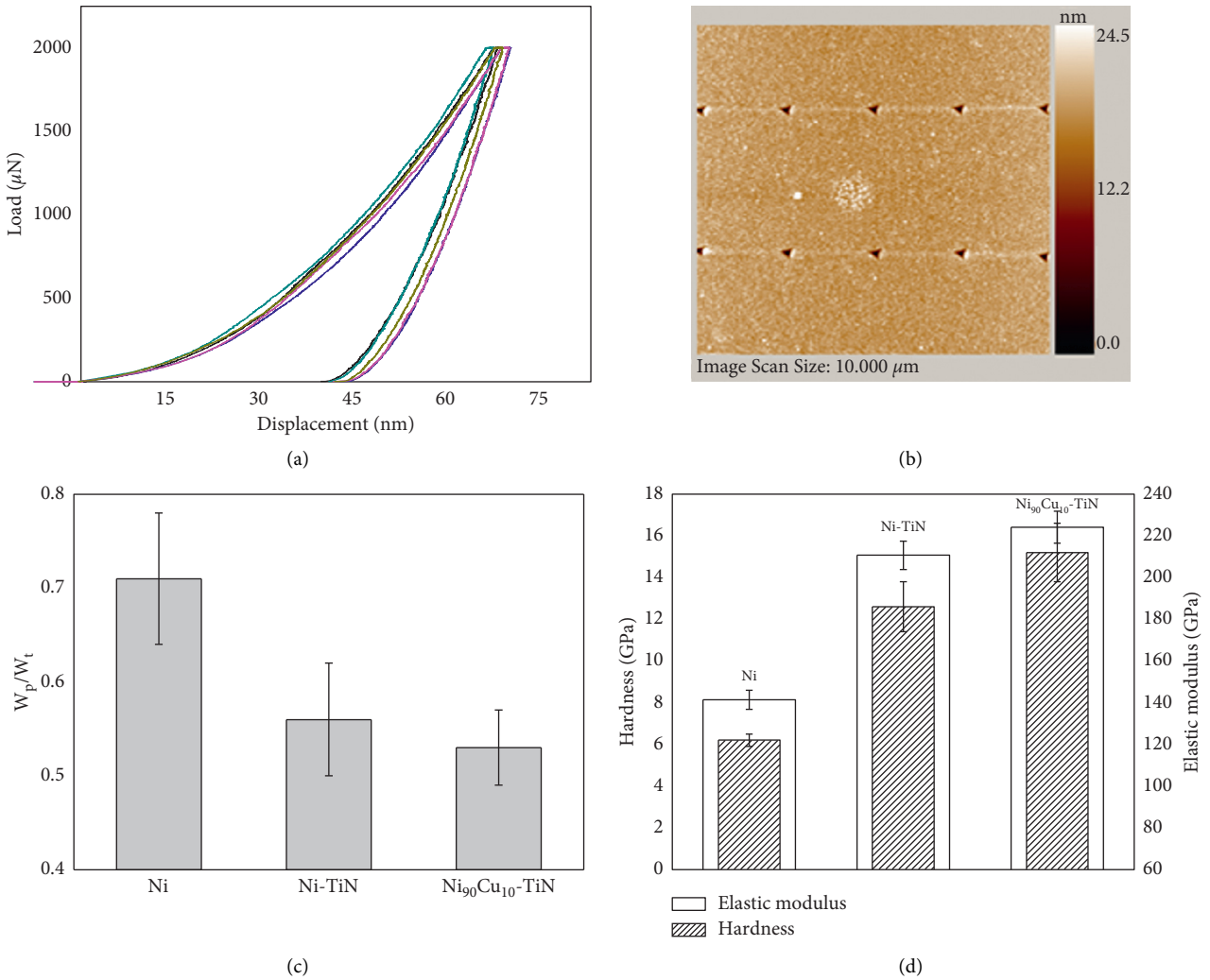

FIGURE 4: (a, b) Load—indentation curve and indentation image of $Ni_{90}Cu_{10}$-TiN, (c) ratio of W_p/W_t, and (d) hardness and elastic modulus of Ni, Ni-TiN, and $Ni_{90}Cu_{10}$-TiN thin films.

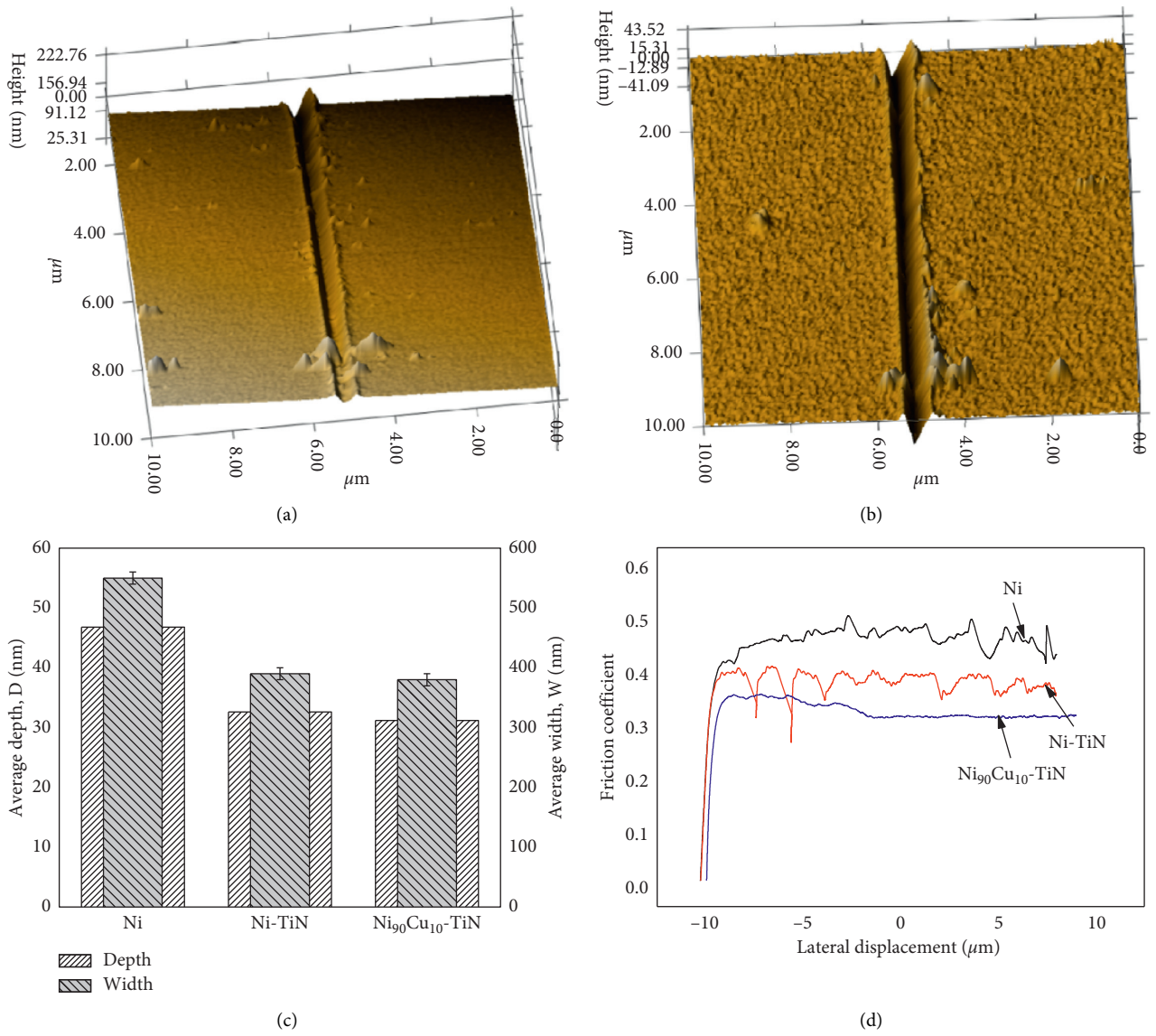

FIGURE 5: (a, b) Surface profile of scratch of Ni-TiN and $Ni_{90}Cu_{10}$-TiN nanocomposite film, (c) depth and width of scratch, and (d) variation of COF with lateral displacement.

observed for the $Ni_{90}Cu_{10}$-TiN and Ni-TiN nanocomposite films is lower than that of pure Ni, which may be due to the observed effects of Cu addition involving both increases in hardness (Figure 5(c)) and decreases in surface roughness. Higher hardness reduces the amount of adhesive interaction between the nanoindenter and the film.

4. Conclusions

A comparative study has been done on microstructure and properties of the nanocrystalline films of pure Ni, Ni-TiN, and $Ni_{90}Cu_{10}$-TiN nanocomposites thin films processed by magnetron cosputtering under optimized conditions. Elastic modulus, nanohardness, and scratch resistance are found to increase with Cu or TiN additions in the nickel matrix. Although a linear proportional relationship between scratch resistance and resistance to plastic deformation is observed, yet the COF values for the nanocomposite films (Ni-TiN and $Ni_{90}Cu_{10}$-TiN) were observed to be less than that of pure Ni.

Data Availability

The data used to support the findings of this work cannot be shared at this moment due to confidential nature of the datasets.

Conflicts of Interest

The authors declare that they have no conflicts of interest.

Acknowledgments

This research was supported by IIT Kharagpur and SGT University, Gurugram, India.

References

[1] E. Marchenko, G. Baigonakova, and Y. Yasenchuk, "Gradient crystalline coating on a biomedical TiNi alloy prepared by magnetron sputtering and annealing," *Vacuum*, vol. 181, Article ID 109652, 2020.

[2] V. Gunther, Y. Yasenchuk, T. Chekalkin et al., "Formation of pores and amorphous-nanocrystalline phases in porous TiNi alloys made by self-propagating high-temperature synthesis (SHS)," *Advanced Powder Technology*, vol. 30, no. 4, pp. 673–680, 2019.

[3] D. Han, H. Yang, M.-S. Kong, C. Lee, A. Sharma, and B. Ahn, "High precision electrolytic polishing of Ni-Ti shape memory alloy for biomedical vascular stents," *Materials Express*, vol. 10, no. 8, pp. 1249–1259, 2020.

[4] Y. Zhao, K. Guo, J. Li, and J. Sun, "Investigation on machinability of NiTi shape memory alloys under different cooling conditions," *International Journal of Advanced Manufacturing Technology*, vol. 116, no. 5-6, pp. 1913–1923, 2021.

[5] Z. G. Li, S. Miyake, M. Kumagai, H. Saito, and Y. Muramatsu, "Hard nanocomposite Ti-Cu-N films prepared by d.c. reactive magnetron co-sputtering," *Surface and Coatings Technology*, vol. 183, no. 1, pp. 62–68, 2004.

[6] A. Akbari, C. Templier, M. F. Beaufort, D. Eyidi, and J. P. Riviere, "Ion beam assisted deposition of TiN-Ni nanocomposite coatings," *Surface and Coatings Technology*, vol. 206, no. 5, pp. 972–975, 2011.

[7] M. Misina, J. Musil, and S. Kadlec, *Surface and Coatings Technology*, vol. 110, p. 168, 1998.

[8] A. Akbari, J. P. Riviere, C. Templier, and E. Le Bourhis, "Structural and mechanical properties of IBAD deposited nanocomposite Ti-Ni-N coatings," *Surface and Coatings Technology*, vol. 200, no. 22-23, pp. 6298–6302, 2006.

[9] A. Akbari, J. P. Riviere, C. Templier, E. L. Bourhis, and G. Abadias, "HARDNESS AND RESIDUAL STRESSES IN TiN-Ni NANOCOMPOSITE COATINGS DEPOSITED BY REACTIVE DUAL ION BEAM SPUTTERING," *Reviews on Advanced Materials Science*, vol. 15, p. 111, 2007.

[10] S. Zhang, D. Sun, Y. Fu, Y. T. Pei, and J. T. M. De Hosson, "Ni-toughened nc-TiN/a-SiNx nanocomposite thin films," *Surface and Coatings Technology*, vol. 200, no. 5-6, pp. 1530–1534, 2005.

[11] P. Karvánková, H.-D. Männling, C. Eggs, and S. Veprek, "Thermal stability of ZrN-Ni and CrN-Ni superhard nanocomposite coatings," *Surface and Coatings Technology*, vol. 146-147, pp. 280–285, 2001.

[12] J. Musil and J. Vlček, "Magnetron sputtering of hard nanocomposite coatings and their properties," *Surface and Coatings Technology*, vol. 142-144, pp. 557–566, 2001.

[13] P. Patsalas, C. Charitidis, S. Logothetidis, C. A. Dimitriadis, and O. Valassiades, "Combined electrical and mechanical properties of titanium nitride thin films as metallization materials," *Journal of Applied Physics*, vol. 86, no. 9, pp. 5296–5298, 1999.

[14] R. Mientus and K. Ellmer, "Reactive DC magnetron sputtering of elemental targets in Ar/N2 mixtures: relation between the discharge characteristics and the heat of formation of the corresponding nitrides," *Surface and Coatings Technology*, vol. 116-119, pp. 1093–1101, 1999.

[15] Y. Igasaki and H. Mitsuhashi, "The effects of substrate bias on the structural and electrical properties of TiN films prepared by reactive r.f. sputtering," *Thin Solid Films*, vol. 70, no. 1, pp. 17–25, 1980.

[16] X. Chu, S. A. Barnett, M. S. Wong, and W. D. Sproul, "Reactive unbalanced magnetron sputter deposition of polycrystalline TiN/NbN superlattice coatings," *Surface and Coatings Technology*, vol. 57, no. 1, pp. 13–18, 1993.

[17] X. Chu, M. S. Wong, W. D. Sproul, and S. A. Barnett, "Mechanical properties and microstructures of polycrystalline ceramic/metal superlattices: TiN/Ni and TiN/Ni0.9Cr0.1," *Surface and Coatings Technology*, vol. 61, no. 1-3, pp. 251–256, 1993.

[18] A. Sharma and B. Ahn, "Microstructural and tribological behavior of pulse electroplated nickel barrier on copper conductors," *Tribology Transactions*, vol. 62, no. 3, pp. 476–485, 2019.

[19] A. Sharma and B. Ahn, "Dry sliding wear behavior of Sn and NiSn overlays on Cu connectors," *Tribology Letters*, vol. 66, no. 136, 2018.

[20] R. Sen, A. Sharma, S. Bhattacharya, S. Das, and K. Das, "Synthesis and characterization of pulse co-electrodeposited nickel/ceria nanocomposites," *Journal of Nanoscience and Nanotechnology*, vol. 10, no. 8, pp. 4998–5003, 2010.

[21] A. M. El-Sherik, U. Erb, G. Palumbo, and K. T. Aust, "Deviations from hall-petch behaviour in as-prepared nanocrystalline nickel," *Scripta Metallurgica et Materialia*, vol. 27, no. 9, pp. 1185–1188, 1992.

[22] L. Benea, P. L. Bonora, A. Borello, and S. Martelli, "Effect of SiC size dimensions on the corrosion wear resistance of the electrodeposited composite coating," *Wear*, vol. 249, no. 10–11, p. 995, 2002.

[23] F.-f. Xia, M.-h. Wu, F. Wang, Z.-y. Jia, and A.-l. Wang, "Nanocomposite Ni-TiN coatings prepared by ultrasonic electrodeposition," *Current Applied Physics*, vol. 9, no. 1, pp. 44–47, 2009.

[24] P. Gyftou, E. A. Pavlatou, and N. Spyrellis, "Effect of pulse electrodeposition parameters on the properties of Ni/nano-SiC composites," *Applied Surface Science*, vol. 254, no. 18, pp. 5910–5916, 2008.

[25] H. Ferkel, B. Müller, and W. Riehemann, "Electrodeposition of particle-strengthened nickel films," *Materials Science and Engineering: A*, vol. 234-236, pp. 474–476, 1997.

[26] A. Möller and H. Hahn, "Synthesis and characterization of nanocrystalline Ni/ZrO2 composite coatings," *Nanostructured Materials*, vol. 12, no. 1-4, pp. 259–262, 1999.

[27] N. Parhizkar, A. Dolati, R. Aghababazadeh, and Z. Lalegani, "Electrochemical deposition of Ni–TiN nanocomposite coatings and the effect of sodium dodecyl sulphate surfactant on the coating properties," *Bulletin of Materials Science*, vol. 39, no. 4, pp. 1021–1027, 2016.

[28] A. Sharma, S. Das, and K. Das, "Pulse electrodeposition of lead-free tin-based composites for microelectronic packaging," *in Electrodeposition of Composite Materials*, pp. 253–274, IntechOpen, London, UK, 2016.

[29] A. Sharma and S. Sharma, "Pulse electrodeposition of lead-free tin-based composites for microelectronic packaging," *in Encyclopedia of Nanoscience and Nanotechnology*, vol. 27, pp. 89–124, American Scientific Publishers, New York, NY, USA, 2018.

[30] M. Kumar, S. Mishra, and R. Mitra, "Effect of Ar:N2 ratio on structure and properties of Ni-TiN nanocomposite thin films processed by reactive RF/DC magnetron sputtering," *Surface and Coatings Technology*, vol. 228, pp. 100–114, 2013.

[31] M. Kumar and R. Mitra, "Effect of substrate bias on microstructure and properties of Ni-TiN nanocomposite thin films deposited by reactive magnetron co-sputtering," *Surface and Coatings Technology*, vol. 251, pp. 239–246, 2014.

[32] M. Kumar and R. Mitra, "Effect of substrate temperature and annealing on structure, stress and properties of reactively co-sputtered Ni-TiN nanocomposite thin films," *Thin Solid Films*, vol. 624, pp. 70–82, 2017.

[33] M. Kumar, "Effect of alloying with Cu and TiN addition on the electrochemical behavior of nanocrystalline Ni processed by magnetron sputtering," *Letters on Materials*, vol. 11, no. 3, pp. 315–320, 2021.

[34] B. D. Cullity, "Elements of X-ray diffraction," Addison-Wesley Publishing Company, Inc., Boston, MA, USA, 1956.

[35] H. Ichimura and I. Ando, "Mechanical properties of arc-evaporated CrN coatings: Part I - nanoindentation hardness and elastic modulus," *Surface and Coatings Technology*, vol. 145, no. 1-3, pp. 88–93, 2001.

[36] P. Panda and R. Ramaseshan, "Effects of Cr doping on the mechanical properties of AlN films grown by the co-sputtering technique," *Ceramics International*, vol. 45, no. 2, pp. 1755–1760, 2019.

[37] P. Panda, N. G. Krishna, P. Rajput, and R. Ramaseshan, "Local crystal structure and mechanical properties of sputtered Ti-doped AlN thin films," *Physical Chemistry Chemical Physics*, vol. 20, no. 47, pp. 29817–29825, 2018.

[38] J. C. Castrillón Trujillo and J. M. Meza Meza, "Deconvolution of design parameters from elasto-plastic energy data acquired by nanoindentation in ceramic coatings," *Scientia et Technica*, vol. 22, no. 2, pp. 131–136, 2017.

[39] G. M. Pharr and A. Bolshakov, "Understanding nano-indentation unloading curves," *Journal of Materials Research*, vol. 17, no. 10, pp. 2660–2671, 2002.

[40] S. R. Bakshi, D. Lahiri, R. R. Patel, and A. Agarwal, *Thin Solid Films*, vol. 518, p. 1701, 2010.

[41] X. M. Liu, Z. L. Liu, and Y. G. Wei, *Tribology Letters*, vol. 46, p. 167, 2012.

[42] S. Bhattacharya, A. Sharma, S. Das, and K. Das, "Synthesis and properties of pulse electrodeposited lead-free tin-based Sn/ZrSiO4 nanocomposite coatings," *Metallurgical and Materials Transactions A*, vol. 47, no. 3, pp. 1292–1312, 2016.

[43] A. Sharma, S. Bhattacharya, S. Das, H.-J. Fecht, and K. Das, "Development of lead free pulse electrodeposited tin based composite solder coating reinforced with ex situ cerium oxide nanoparticles," *Journal of Alloys and Compounds*, vol. 574, pp. 609–616, 2013.